Vortex dynamics in thin films of $YBa_2Cu_3O_{7-x}$ with three-dimensional nanoscale patterns

J. Gutierrez,[1] A. Palau,[2] J. H. Durrell,[2] N. Romà,[1] T. Puig,[1] X. Obradors,[1] and M. G. Blamire[2]
[1]*Institut de Ciència de Materials de Barcelona, CSIC, Campus de la UAB, 08193 Bellaterra, Spain*
[2]*Department of Materials Science, University of Cambridge, Pembroke Street, Cambridge, CB2 3QZ, United Kingdom*
(Received 14 October 2008; revised manuscript received 7 January 2009; published 26 February 2009)

We have machined vertical transport structures in YBCO thin films in which the current is constrained to flow along the *c* axis. When current is forced to flow outside the *a-b* planes in YBCO a component of the Lorentz force arises acting along them. Consequently we have been able to directly measure the magnitude of the pinning force acting on vortices moving within the *a-b* planes, and demonstrate vortex cutting, vortex channeling, and pinning by twin boundaries. Such measurements are not otherwise possible in *c*-axis films. We show that vortex channeling can be inhibited by a Lorentz force component acting perpendicularly to the channel. This is ascribed to pinning of the vortices within the channel by the channel wall.

DOI: 10.1103/PhysRevB.79.064526 PACS number(s): 74.25.Qt, 47.32.C−, 62.23.St

I. INTRODUCTION

The key issue for the comprehension of vortex matter in high-T_c superconductors (HTS) has been the proper understanding of vortex-vortex and vortex-defect interactions on these materials. Studies of pinning mechanisms and methods to enhance their effectiveness in HTS are a topic of great interest, especially in technologically relevant materials such as $YBa_2Cu_3O_{7-x}$ (YBCO) thin films. In such films several different types of defects are present and their contribution to the pinning energy is difficult to isolate. Although many defects can act as effective pinning sites, it has been demonstrated that cutting and channeling processes occur in inhomogeneous superconductors with strong and weak pinning regions, such us grain boundaries,[1] twin boundaries,[2] or *a-b* planes,[3,4] determining the critical current over a substantial range of magnetic field angles. Vortex cutting and recombination represent a mechanism for bypassing pinning centers.[5,6] Moreover, in YBCO, *a-b* plane vortex channeling is expected to occur in any thin or thick film where the current flow is not entirely aligned with the planes, potentially strongly reducing the critical current density. There has been much interest in developing artificial nanoscale vortex channels to guide vortices for studies of vortex matter in confined geometries[6–8] and for fabrication of vortex ratchets where, if a suitable asymmetric pinning potential is chosen, vortices will preferentially move in one direction.[9,10] Understanding of cutting and channeling processes will be particularly important for magnet applications of HTS where complex magnetic field orientations have to be used.

We have nanofabricated structures in *c*-axis YBCO thin films, which allows us to apply current perpendicular to the *a-b* planes, and by rotating the magnetic field, both in-plane and out-of-plane, we can study the pinning forces that control vortex channeling along the *a-b* planes and the effect of other defects acting as in-plane pinning centers. Such defects can remain masked in conventional experiments where the current is constrained to flow only along the *a-b* planes. With this configuration we have been able to measure the *a-b* plane cutting and channeling forces in YBCO with an experimental geometry that allows us to resolve the interconnected contribution of the Lorentz force ($\boldsymbol{F_L}=\boldsymbol{J_c}\times\boldsymbol{B}$) and anisotropy. With this particular geometry we have been able to identify channeling suppression through interaction of vortices with the channel sidewalls under the action of a Lorentz force perpendicular to the channels.

II. EXPERIMENTAL DETAILS

YBCO thin films with thicknesses $t\sim 550$ nm were grown on $LaAlO_3$ single-crystal substrates using a trifluoroacetate (TFA) precursor route.[11,12] X-ray diffraction analysis showed (001)-oriented films with a typical rocking curve width of the (005) peak $<0.5°$ and in-plane orientation spread $<1°$, indicative of good crystallographic alignment. Samples were patterned with contact pads and 4 μm wide tracks using photolithography and Ar-ion milling. Contacts were prepared by sputtering Ag/Au bilayers. Structures with vertical transport structures were fabricated with a three-dimensional milling technique[13] by using a FEI FIB200 Focused Ion Beam (FIB) system. In that system the sample holder could be rotated about an axis collinear with film track between $\beta=0°$ (beam incidence normal to the substrate) and 90° (beam incidence parallel to the substrate). Figure 1(a) shows a schematic representation of typical structure geometry. To fabricate the structures, we first narrowed the 4 μm tracks down to $k\sim 600$ nm with $\beta=0°$ by using 70 pA and 30 kV beam. Sidewalls were cleaned with low-energy beam in order to minimize the amount of gallium spread over the surface of the sample. Lateral cuts were made at low-energy beam by tilting the sample with $\beta\sim 85°$ leaving a longitudinal dimension, *l*. In order to constrain the current flow along the *c* axis we overlapped the two lateral cuts by *x*. With this configuration the theoretical current flow will be tilted from the *a-b* plane by an angle $\alpha=\arctan(x/l)$. Here, by changing the overlapping distance, we can modify the current direction in the structure and thus have a complete control of the resultant Lorentz force. Other experiments with a current component along the *c* axis were performed in vicinal films.[3,4] However, in those experiments, the maximum tilt angle for the current was restricted to $\alpha<10°$ since for larger substrate misorientations it was not possible to grow good quality films. This experimental technique allows a larger range of α values and thus a good

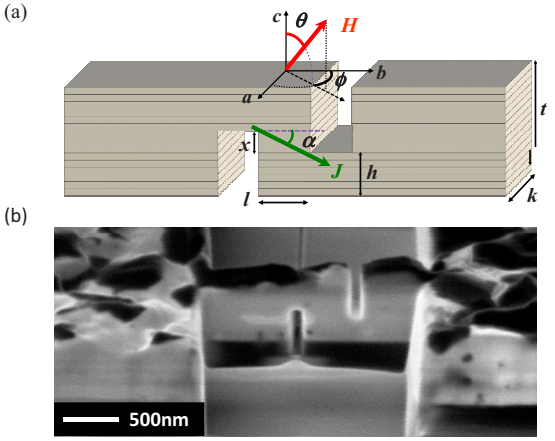

FIG. 1. (Color online) (a) Schematic diagram of the experimental structure fabricated by focused ion beam (FIB) with the angle of the applied field and the current indicated. (b) FIB picture of a standard YBCO structure patterned into the same geometry.

control of the F_L direction, which will drive vortices along the *a-b* planes (in-plane motion). All the structure dimensions and the ion source energies used were accurately optimized to prevent a damage of YBCO induced by the gallium ions during milling process. The key factor was the balance between time of milling and beam current. To maximize the tilting angle, α, to prevent a potential sample damage, and to assure a good structural stability, a compromise between the transverse and longitudinal dimensions had to be found. As an optimum we set $l \sim 450$ nm and $h \geq 120$ nm. With these conditions, we performed structures with α values going from $\alpha \sim 3°$ to $\alpha \sim 30°$. However, higher α values could be attained by using thicker samples.

Figure 1(b) shows a FIB image of a typical structure fabricated using this process. The T_c of the samples was checked before and after the milling. It remained the same, $T_c \sim 90$ K. Similar three-dimensional (3D) nanostructures have been used to study multilayers with different magnetic or superconducting properties on low-temperature superconductors.[6,13,14]

III. EXPERIMENTAL RESULTS AND DISCUSSION

Angle-dependent critical current density, J_c, was measured using a two-axis goniometer mounted in an 8 T cryostat by rotating the magnetic field in plane (ϕ) and out of plane (θ) of the film [see Fig. 1(a)]. A schematic representation of the measurement geometries used in this work is presented in Fig. 2. Figures 2(a) and 2(b) show a representation of the out-of-plane rotations, while Figs. 2(c) and 2(d) show the variation in the Lorentz force during an in-plane scan. Critical current values were determined using a criterion of 0.5 μV.

A. Out-of-plane rotations at $\phi=0°$: in-plane confined F_L

First of all we have performed $J_c(\theta)$ measurements at $\phi=0°$, i.e., rotating the magnetic field out of plane along the current track [see Fig. 2(a)]. Figure 3 shows $J_c(\theta)$ data taken

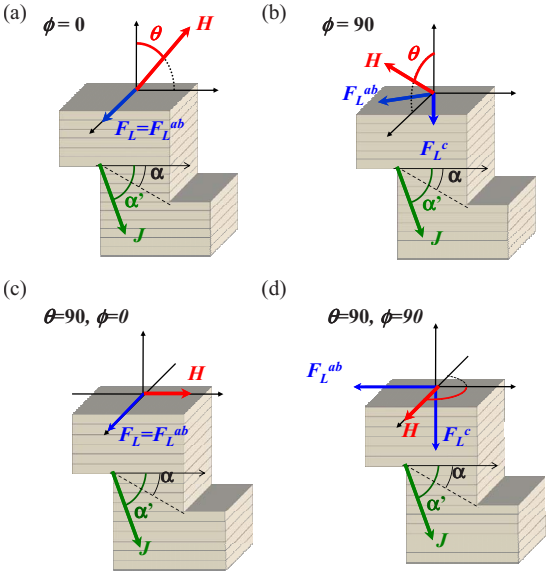

FIG. 2. (Color online) Schematic diagram of the different measurement geometries used in this work with the effective current tilt angle, α', indicated. (a) Out-of-plane rotation along the current track. (b) Out-of-plane rotation perpendicular to the current track. (c) Representation of the Lorentz force direction for $\theta=90°$ and $\phi=0°$. (d) Representation of the Lorentz force direction for $\theta=90°$ and $\phi=90°$.

at $\phi=0°$, $T=50$ K, and $H=1$ T for YBCO structures with $\alpha \sim 6° \pm 0.5°$ [Fig. 3(a)] and $\alpha \sim 30° \pm 2°$ [Fig. 3(b)]. For comparison purposes we have also included the $J_c(\theta)$ dependence obtained for a full track with $\alpha=0°$ measured under the same conditions. Since in the latter case dissipation arises due to current flowing along the *a-b* planes, we obtained larger J_c values than that measured for the structures with $\alpha \neq 0°$, where dissipation comes from current flowing along the *c* axis. The reduction observed is in agreement with the expected decrease in J_c due to the YBCO anisotropy, i.e., $J_c^{ab} \sim \gamma J_c^c$,[15] where J_c^c and J_c^{ab} are the critical current values along the *c* axis and the *a-b* planes, respectively, and $\gamma \sim 5-7$ is the YBCO electron mass anisotropy.[16] We have also considered this anisotropy to determine the effective tilt of the current flow, α', in each structure, as $\alpha' = \arctan(\gamma x/l)$. Considering $\gamma \sim 5$ we obtain $\alpha' \sim 70° \pm 3°$ and $\alpha' \sim 30° \pm 2°$ for the structure with $\alpha \sim 30° \pm 2°$ and $\alpha \sim 6° \pm 0.5°$, respectively (see Fig. 2). It should be noted that the current flow direction is an averaged value and the errors in α take this into account.

The rotations performed at $\phi=0°$ induce an in-plane Lorentz force, F_L^{ab}, i.e., there is no F_L component perpendicular to the planes. The following equation gives the angular dependence of F_L:

$$F_L = F_L^{ab}(\phi=0) = J_c B|\sin\theta \sin\alpha' + \cos\theta \cos\alpha'|. \quad (1)$$

The sharp peak observed at $\theta = \pm 90°$ for the sample with $\alpha=0°$ arises basically from the YBCO anisotropy together with the contribution of the force-free (FF) effect at the same position (F_L goes to zero at $\theta = \pm 90°$). By introducing a small current tilt angle in the structure, $\alpha \sim 6° \pm 0.5°$ (α'

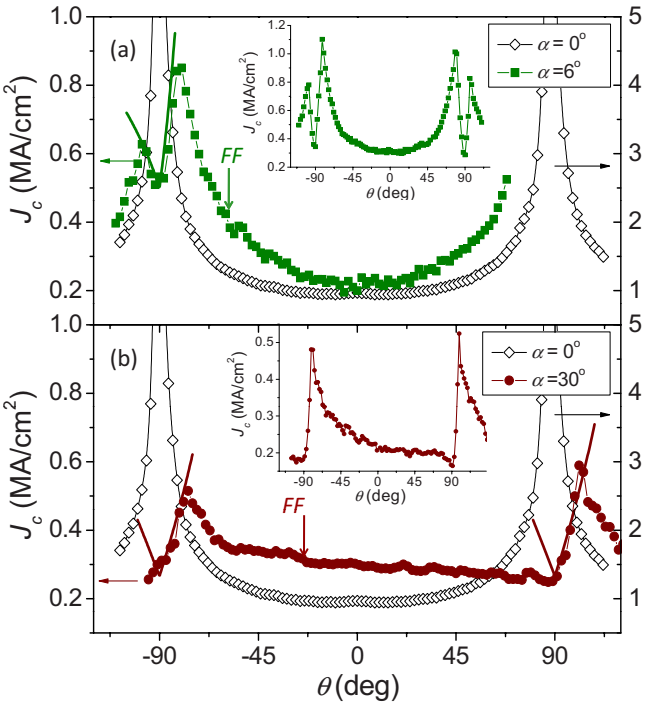

FIG. 3. (Color online) $J_c(\theta)$ dependence measured at $\phi=0°$, $T=50$ K, and $\mu_0 H=1$ T for YBCO structures with (a) $\alpha \sim 6° \pm 0.5°$ ($\alpha' \sim 30° \pm 2°$) and (b) $\alpha \sim 30° \pm 2°$ ($\alpha' \sim 70° \pm 3°$). Open symbols show $J_c(\theta)$ values obtained for a YBCO track with $\alpha=0°$ at the same conditions. Solid lines are theoretical fits to the experimental data using Eq. (2). Inset to Fig. 3(a) shows the $J_c(\theta)$ dependence measured at $\phi=0°$, $T=25$ K, and $\mu_0 H=2$ T for the structure with $\alpha \sim 6° \pm 0.5°$. Inset to Fig. 3(b) shows the $J_c(\theta)$ dependence measured at $\phi=0°$, $T=50$ K, and $\mu_0 H=2$ T for the structure with $\alpha \sim 30° \pm 2°$.

$\sim 30° \pm 2°$), we move the force-free position to $\theta \sim -60°$, inducing a notable broadening of the $-90°$ peak which in this case is mostly associated with the YBCO anisotropy [Fig. 3(a)]. However, the most important feature that has to be noticed is the appearance of a strong minimum in J_c *at* $\theta=-90°$. It is associated with the in-plane easy motion of vortices when the magnetic field is aligned with the *a-b* planes. Inset to Fig. 3(a) shows $J_c(\theta)$ data taken at $T=25$ K and $H=2$ T for the same structure with $\alpha' \sim 30° \pm 2°$. In this case we can see the corresponding minima at $\theta= \pm 90°$.

Vortex channeling between the *a-b* planes appears since by introducing a *c*-axis component in the current flow ($\alpha' \neq 0°$) there is always a nonzero F_L^{ab} value at $\theta= \pm 90°$. The J_c decrease at the channeling minima ($\theta= \pm 90°$) is enhanced as the *c*-axis current and the associated F_L^{ab} grow. This enhancement has been observed by increasing the tilting angle, $\alpha' \sim 70° \pm 3°$ [Fig. 3(b)] and thus the value of $F_L^{ab} = J_c B|\sin \alpha'|$. For this particular structure with $\alpha' \sim 70° \pm 3°$ the force-free peak is shifted to $\theta \sim -30°$, inducing an asymmetric $J_c(\theta)$ dependence around $\theta \sim 0°$. The peak observed at $\theta= \pm 90°$ is only associated with the YBCO anisotropy. Again, this peak is truncated at $\theta= \pm 90°$ due to vortex channeling along the *a-b* planes. Inset to Fig. 3(b) shows the $J_c(\theta)$ dependence obtained at 50 K and 2 T where the channeling minima at $\theta= \pm 90°$ can be clearly identified.

Considering that, close to the channeling minima, vortex motion occurs after vortex cutting and channeling along *a-b* planes,[3,4] the F_L balance equation can be written as $f_L = f_{\text{pin}}^{ab} + f_{\text{cut}}/L$, where f_L is the Lorentz force per unit length, f_{pin}^{ab} is the pinning force of the vortex segments within the *a-b* planes per unit length, f_{cut} is the force required to cut and cross-join a single vortex, and L is the length of each vortex segment in the *a-b* planes. Then, considering the measurement geometry $L=d/|\cos \theta|$, where $d \sim 0.39$ nm is the spacing between YBCO *a-b* planes,[3] the $J_c(\theta)$ behavior at $\phi=0°$ can be written as

$$J_c(\phi=0) = \frac{f_{\text{pin}}^{ab} + (f_{\text{cut}}|\cos \theta|/d)}{\Phi_0 |\sin \theta \sin \alpha' + \cos \theta \cos \alpha'|}. \quad (2)$$

Equation (2) was used for fitting the experimental $J_c(\theta)$ data in Fig. 3 near the channeling minima ($\theta= \pm 90°$) at $T=50$ K and $H=1$ T for the two structures with different α' (solid lines). We obtained $f_{\text{pin}}^{ab}=5.10^{-6}$ N/m and $f_{\text{cut}}=8.0^{-15}$ N, values similar to those obtained in vicinal films.[3]

It is worth noting that the whole $J_c(\theta)$ curve is reduced by a factor of 5 even for very small current tilt angles, such as $\alpha \sim 6° \pm 0.5°$. The J_c values at the channeling minima, $\theta= \pm 90°$, are even more reduced, i.e., $J_c^{\alpha=0}(\theta= \pm 90°)/J_c^{\alpha \approx 6}(\theta= \pm 90°) \sim 13$ and $J_c^{\alpha=0}(\theta= \pm 90°)/J_c^{\alpha \approx 30}(\theta= \pm 90°) \sim 24$. This can be understood by assuming that vortices easily flow along the *a-b* planes when the magnetic field is applied parallel to them.[4]

B. Out-of-plane rotations at $\phi=90°$: in-plane and out-of-plane F_L

The present measurements show that our structures allow the investigation of the in-plane vortex motion. With the F_L completely directed along the *a-b* planes the vortex motion seems to be governed by vortex cutting and channeling processes described in Eq. (2). Flux cutting and channeling experiments have also been performed in the geometry with the magnetic field applied at $\phi=90°$, i.e., rotating the magnetic field perpendicular the current track [see Fig. 2(b)]. In this case there is a component of the F_L directed perpendicular to the *a-b* planes, F_L^c,

$$F_L^c(\phi=90) = J_c B|\sin \theta \cos \alpha'|. \quad (3)$$

Figure 4(a) shows $J_c(\theta)$ data measured at $T=50$ K and $H=1$ T for $\phi=0°$ on the structure with $\alpha \sim 30° \pm 2°$ [presented in Fig. 3(b)] compared with the same scan performed at $\phi=90°$. A schematic representation of the F_L induced at the channeling position ($\theta=90°$) for $\phi=0°$ and $\phi=90°$ is shown in Figs. 2(c) and 2(d), respectively.

For this particular configuration the current flows with a very large tilt angle $\alpha' \sim 70° \pm 3°$, resulting in a small F_L^c component pushing vortices normal to the *a-b* planes. [see Eq. (3)]. A pronounced J_c minimum at $\theta= \pm 90°$ for both $\phi=0°$ and $\phi=90°$ [Fig. 4(a)] so that the channeling minima do not change by introducing a small F_L^c component. A very different situation is seen in the structure performed with a small current tilt angle, $\alpha \sim 4° \pm 0.5°$ ($\alpha' \sim 20° \pm 1°$), i.e.,

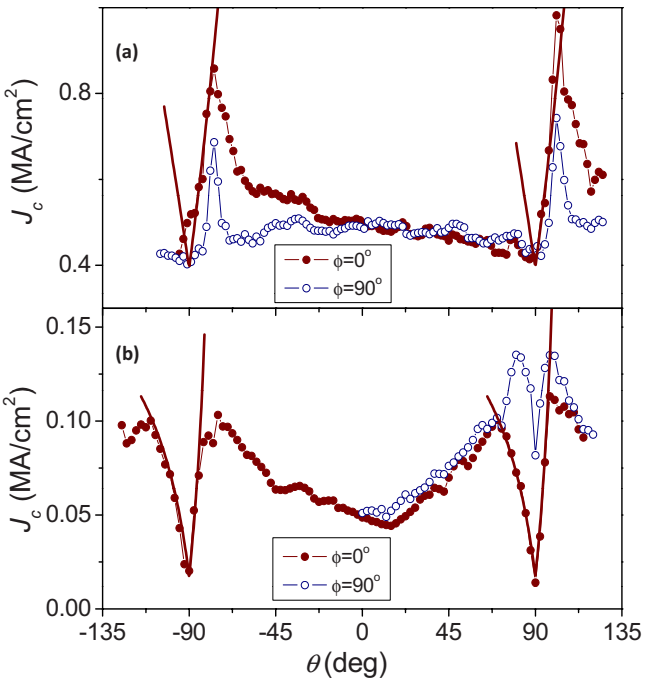

FIG. 4. (Color online) $J_c(\theta)$ dependence measured at $\phi=0°$ (solid symbols) and $\phi=90°$ (open symbols) for (a) a structure with $\alpha\sim30°\pm2°$ ($\alpha'\sim70°\pm3°$) at $T=50$ K and $\mu_0H=1$ T and (b) a structure with $\alpha\sim4°\pm0.5°$ ($\alpha'\sim20°\pm1°$) at $T=60$ K and $\mu_0H=2$ T. Solid lines are theoretical fits to the experimental data using Eq. (2)

with a large F_L^c component, shown in Fig. 4(b). In this case, the channeling minima measured in the θ scan performed at $T=60$ K and $H=2$ T for $\phi=0°$ can be accurately fitted with Eq. (1) with $f_{\text{pin}}^{ab}=1.2.10^{-7}$ N/m and $f_{\text{cut}}=1.4.10^{-15}$ N (solid lines). These values are smaller than the ones obtained at 50 K and 1 T [Figs. 3 and 4(a)] as expected since both f_{pin}^{ab} and f_{cut} decrease with increasing the temperature.[6] However, the channeling minima clearly depend on the field angle in the plane of the film, ϕ, being less pronounced for the scan performed at $\phi=90°$. Thus, we observe that introducing a large F_L component directed normal to the a-b planes (i.e., reducing the tilting current angle α' [see Eq. (3)]) in-plane vortex channeling is hampered.

C. In-plane rotations at $\theta=90°$

In order to study vortex channeling dependence on F_L^c, we measured $J_c(\phi)$ at the channeling minima ($\theta=90°$) for the structure with $\alpha\sim4°\pm0.5°$, where by rotating the magnetic field in plane we can induce a large F_L^c component. Figure 5 shows the data measured at $T=65$ K and $H=1$ T. In this configuration F_L^{ab} remains constant over the entire scan and F_L^c depends on ϕ as

$$F_L^c(\theta=90)=J_cB|\sin\varphi\cos\alpha'|, \tag{4}$$

being zero at $\phi=0°$ [Fig. 2(c)] and maximum at $\theta=\pm90°$ [Fig. 2(d)].

From this $J_c(\phi)$ behavior it is clear that the J_c value at the channeling minima increases with increasing F_L^c, which suggests that vortex channeling is inhibited when there is a considerable component of the Lorentz force pushing vortices against the a-b planes. In order to evaluate the blocking force acting to inhibit vortex channeling, we have considered that an effective friction force per unit length, f_{fr}, exist in the Lorentz force balance along the a-b planes, $F_L^{ab}=J_cB|\sin\alpha'|$, acting against vortex channeling, i.e., $F_L^{ab}=F_{\text{pin}}^{ab}+F_{\text{fr}}$. Since the friction force is proportional to the force normal to the movement direction we have $F_{\text{fr}}=\mu F_L^c$, where μ is the friction coefficient and by using Eq. (4) we obtain the following $J_c(\phi)$ dependence:

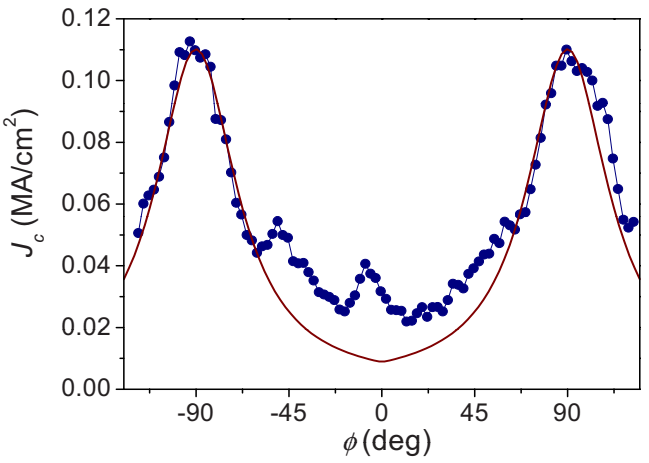

FIG. 5. (Color online) $J_c(\phi)$ dependence measured at the channeling minima ($\theta=90°$) for a structure with $\alpha\sim4°\pm0.5°$ ($\alpha'\sim20°\pm1°$) at $T=65$ K and $\mu_0H=1$ T. Solid line shows the theoretical fit obtained using Eq. (5).

$$J_c^{\theta=\pm90}=\frac{f_{\text{pin}}^{ab}}{\Phi_0|\sin\alpha'-\mu|\sin\phi\cos\alpha'||}. \tag{5}$$

Equation (5) has been used to fit the experimental data shown in Fig. 5 with $f_{\text{pin}}^{ab}=7.10^{-8}$ N/m and $\mu=0.33$. Although we have considered a very simple model to introduce the effect of F_L^c on in-plane vortex channeling, Eq. (5) reproduce well the general trend observed in the experimental data (solid line), providing an evidence that channeling along a-b planes can be precluded by introducing enough force directed normal to the planes, without reducing the in-plane force component.

Measuring the $J_c(\phi)$ dependence at $\theta\sim90°$, i.e., with magnetic field in the plane of the film, we can study in-plane vortex motion and thus in-plane vortex pinning defects acting against vortex channeling. This is elucidated by the data shown in Fig. 5. We observe a clear increase in J_c at around $\phi=\pm45°$, corresponding to the alignment of magnetic field with YBCO twin boundaries (located along the [110] and [−110] directions[2]). This indicates that at 65 K and 1 T vortex channeling is reduced due to the pinning produced by the twin boundaries. While the peak around −45° (corresponding to the [−110] family) appears well defined the peak at 45° is less pronounced. This asymmetry could arise due to a smaller presence of twin boundaries corresponding to the [110] family. A macroscopic study is not expected to find

such a difference but the structures used in this work are small enough (compared to the size and distribution of the twin boundaries[2]) to contain a significant different number of twin boundaries from one of the two families.. We also observe a peak at $\phi=0°$, which is probably due to surface pinning when magnetic field is applied parallel to the lateral cuts of the track.

IV. CONCLUSION

In conclusion, we have successfully patterned 3D nanostructures on YBCO films by FIB without T_c reduction. By changing the geometry of the structures, we were able to tune the Lorentz force component parallel and perpendicular to the *a-b* planes and thus study vortex dynamics within the CuO_2 planes. In particular, we have found that easy vortex motion through low pinning channels can be controlled and slowed down by applying enough force perpendicular to the channels. The nanofabricated nature of our structures allows for future explorations of the *c*-axis electrical transport properties, pinning force, and the vortex channeling along the *a-b* planes, which is otherwise impossible in *c*-axis films. Moreover, the effect of anisotropic defects on the in-plane vortex motion can be easily studied.

ACKNOWLEDGMENTS

This work was supported by the U.K. EPSRC, MEC (FPU and MAT2005-02047), and EU (HIPERCHEM, NESPA).

[1] J. H. Durrell, M. J. Hogg, F. Kahlmann, Z. H. Barber, M. G. Blamire, and J. E. Evetts, Phys. Rev. Lett. **90**, 247006 (2003).
[2] A. Palau, J. H. Durrell, J. L. MacManus-Driscoll, S. Harrington, T. Puig, F. Sandiumenge, X. Obradors, and M. G. Blamire, Phys. Rev. Lett. **97**, 257002 (2006).
[3] J. H. Durrell, G. Burnell, V. N. Tsaneva, Z. H. Barber, M. G. Blamire, and J. E. Evetts, Phys. Rev. B **70**, 214508 (2004).
[4] P. Berghuis, E. DiBartolomeo, G. A. Wagner, and J. E. Evetts, Phys. Rev. Lett. **79**, 2332 (1997).
[5] A. Schonenberger, A. Larkin, E. Heeb, V. Geshkenbein, and G. Blatter, Phys. Rev. Lett. **77**, 4636 (1996).
[6] A. Palau, R. Dinner, J. H. Durrell, and M. G. Blamire, Phys. Rev. Lett. **101**, 097002 (2008).
[7] A. Pruymboom, P. H. Kes, E. van der Drift, and S. Radelaar, Phys. Rev. Lett. **60**, 1430 (1988).
[8] N. Kokubo, R. Besseling, V. M. Vinokur, and P. H. Kes, Phys. Rev. Lett. **88**, 247004 (2002).
[9] D. Cole, S. Bending, S. Savel'ev, A. Grigorenko, T. Tamegai, and F. Nori, Nat. Mater. **5**, 305 (2006).
[10] K. Yu, T. W. Heitmann, C. Song, M. P. Defeo, B. L. T. Plourde, M. B. S. Hesselberth, and P. H. Kes, Phys. Rev. B **76**, 220507 (2007).
[11] N. Roma, S. Morlens, S. Ricart, K. Zalamova, J. M. Moreto, A. Pomar, T. Puig, and X. Obradors, Supercond. Sci. Technol. **19**, 521 (2006).
[12] X. Obradors, T. Puig, A. Pomar, F. Sandiumenge, N. Mestres, M. Coll, A. Cavallaro, N. Roma, J. Gazquez, J. C. Gonzalez, O. Castano, J. Gutierrez, A. Palau, K. Zalamova, S. Morlens, A. Hassini, M. Gibert, S. Ricart, J. M. Moreto, S. Pinol, D. Isfort, and J. Bock, Supercond. Sci. Technol. **19**, S13 (2006).
[13] C. Bell, G. Burnell, D. J. Kang, R. H. Hadfield, M. J. Kappers, and M. G. Blamire, Nanotechnology **14**, 630 (2003).
[14] J. W. A. Robinson, S. Piano, G. Burnell, C. Bell, and M. G. Blamire, Phys. Rev. Lett. **97**, 177003 (2006).
[15] G. Blatter, M. V. Feigel'man, V. B. Geshkenbein, A. I. Larkin, and V. M. Vinokur, Rev. Mod. Phys. **66**, 1125 (1994).
[16] U. Welp, W. K. Kwok, G. W. Crabtree, K. G. Vandervoort, and J. Z. Liu, Phys. Rev. Lett. **62**, 1908 (1989).